Physics Letters B 791 (2019) 242–248

Contents lists available at ScienceDirect

Physics Letters B

www.elsevier.com/locate/physletb

Energy and momentum dependence of nuclear short-range correlations - Spectral function, exclusive scattering experiments and the contact formalism

Ronen Weiss [a,*], Igor Korover [b], Eli Piasetzky [c], Or Hen [d], Nir Barnea [a]

[a] The Racah Institute of Physics, The Hebrew University, Jerusalem, Israel
[b] Department of Physics, NRCN, P.O.B. 9001, Beer-Sheva 84190, Israel
[c] School of Physics and Astronomy, Tel Aviv University, Tel Aviv 69978, Israel
[d] Massachusetts Institute of Technology, Cambridge, MA 02139, USA

ARTICLE INFO

Article history:
Received 20 July 2018
Received in revised form 10 February 2019
Accepted 15 February 2019
Available online 19 February 2019
Editor: W. Haxton

Keywords:
Short range correlations
Electron scattering
Spectral function
Contact formalism

ABSTRACT

Results of electron-induced one- and two-nucleon hard knockout reactions, $A(e,e'p)$ and $A(e,e'pN)$, in kinematics sensitive to nuclear short-range correlations, are studied using the nuclear contact formalism. A relation between the spectral function and the nuclear contacts is derived and used to analyze the dependence of the data on the initial energy and momentum of the knocked-out proton. The ratio between the number of emitted proton-proton pairs and proton-neutron pairs is shown to depend predominantly on a single ratio of contacts. This ratio is expected to present deep minima in the initial energy and momentum plane, associated with the node in the proton-proton wave function.

The formalism is applied to analyze data from recent ^{4}He and ^{12}C electron-scattering experiments performed at Jefferson laboratory. Different nucleon-nucleon potentials were used to assess the model-dependence of the results. For the ratio of proton-proton to proton-neutron pairs in ^{4}He, a fair agreement with the experimental data is obtained using the two potentials, whereas for the ratio of proton-proton pairs to the total knocked-out protons in ^{12}C, some of the features of the theory are not seen in the experimental data. Several possible explanations for this disagreement are discussed. It is also observed that the spectral function at specific domains of the momentum-energy plane is sensitive to the nucleon-nucleon interaction. Based on this sensitivity, it might be possible to constrain the short range part of the nuclear potential using such experimental data.

In order to fully describe nuclear systems, it is necessary to understand the short-range behavior of interacting nucleons, i.e. the implications of few nucleons being close to each other inside the nucleus. These nuclear short-range correlations (SRCs) have been studied intensively in the last decades. High-energy and large momentum-transfer electron and proton-scattering experiments show that almost all of the nucleons with momentum larger than the Fermi momentum are part of an SRC pair, which amount to about 20% of the nucleons in medium-size and heavy nuclei [1–9]. A dominance of neutron-proton pairs was observed among the different possible pairs [5–11]. These conclusions are also supported by theoretical works, in which ab-initio calculations of momentum distributions in nuclei show a universal high-momentum tail, similar in shape to the deuteron high-momentum tail [12–17]. For more details, see recent reviews [18,19].

Recently, the nuclear contact formalism, a new approach for analyzing nuclear SRCs, was presented [20–23]. In this theory, new parameters, called the nuclear contacts, describe the probability of finding two nucleons close to each other inside the nucleus. The values of these contacts depend on the specific nucleus discussed. Another important ingredients of this theory are the universal two-body functions that describe the motion of the SRC pairs. These functions can be model-dependent, i.e. depend on the nucleon-nucleon interaction, however they are identical for all nuclei. This theory was used previously to derive the nuclear contact relations, which are relations between the nuclear contacts and different nuclear quantities, such as the one-body and two-body momentum and coordinate space distributions [21,23], the photo-absorption cross section [20,24], the Coulomb sum rule [25], and the correlation function [26].

* Corresponding author.
E-mail addresses: ronen.weiss1@mail.huji.ac.il (R. Weiss), nir@phys.huji.ac.il (N. Barnea).

https://doi.org/10.1016/j.physletb.2019.02.019

The purpose of this paper is to study and analyze electron-scattering experimental data using the contact theory. We will focus on hard semi-exclusive and exclusive scattering experiments, in which one or two emitted nucleons are measured in addition to the scattered electron [7–9,27–29]. These measurements, in appropriate kinematics, are one of the main experimental methods for studying nuclear SRCs, and thus it is important to have a good theoretical description of their results.

In electron-scattering experiments, under the one-photon exchange approximation, momentum $\boldsymbol{q}$ and energy ω are transferred to the nucleus by a virtual photon. If $Q^2 \equiv q^2 - \omega^2$ is large enough ($\gtrsim 1.5$ GeV^2), the photon is predominantly absorbed by a single nucleon. This nucleon is knocked out from the nucleus and its momentum $\boldsymbol{p}_1'$ and energy ϵ_1' are measured. Neglecting final-state interaction (FSI), the initial momentum and (off-shell) energy $(\boldsymbol{p}_1, \epsilon_1)$ of the nucleon in the nucleus ground state, before it was knocked out, can be reconstructed

$$\boldsymbol{p}_1 = \boldsymbol{p}_1' - \boldsymbol{q}, \qquad \epsilon_1 = \epsilon_1' - \omega. \tag{1}$$

If the initial momentum p_1 is larger than the typical Fermi momentum $p_F \approx 255$ MeV/c $= 1.3$ fm^{-1}, then it is most likely that the knocked-out nucleon was part of an SRC pair. In this case, an emission of a second nucleon is to be expected. This nucleon is the correlated partner. Its final momentum $\boldsymbol{p}_2'$ equals its initial-state momentum inside the nucleus $\boldsymbol{p}_2 = \boldsymbol{p}_2'$.

This description indicates that the semi-exclusive and exclusive cross sections should be proportional to the probability of finding a nucleon with momentum $\boldsymbol{p}_1$ and energy ϵ_1 in the initial state, which is just the definition of the spectral function $S^N(\boldsymbol{p}_1, \epsilon_1)$. Indeed, it was shown in [30] that within the plane-wave impulse approximation (PWIA), the $(e, e'N)$ cross section is given by

$$\frac{d^4\sigma}{d\Omega_{k'} d\epsilon_k' d\Omega_{p_1'} d\epsilon_1'} = p_1' \epsilon_1' \sigma_{eN} S^N(\boldsymbol{p}_1, \epsilon_1) \tag{2}$$

where, $k'_\mu = (\boldsymbol{k}', \epsilon_k')$ is the final electron four-momentum, N denotes a knocked-out neutron or a proton, and σ_{eN} is the off-shell electron-nucleon cross section.

In the case of high-Q^2 two nucleon knockout reactions, previous theoretical [17,31,32] and experimental [6] studies have shown that the measured cross-section can be factorized in a similar manner to Eq. (2), replacing the one-body spectral function by the two-body decay function $D_A(\boldsymbol{p}_1, \boldsymbol{p}_2, E_R)$. The latter represents the probability for a hard knockout of a nucleon with initial momentum $\boldsymbol{p}_1$, followed by an emission of a recoil nucleon with momentum $\boldsymbol{p}_2$. E_R is the energy of the $A-1$ system, composed of nucleon 2 and the residual $A-2$ nucleus. We note that integrating the decay function over all recoil nucleon momenta $(\boldsymbol{p}_2)$ yields the spectral function.

Under few simple assumptions, which will be presented below, the asymptotic high-momentum proton spectral function can be written as

$$\begin{aligned} S^p(p_1, \epsilon_1) = {} & C_{pn}^1 S_{pn}^1(p_1, \epsilon_1) + C_{pn}^0 S_{pn}^0(p_1, \epsilon_1) \\ & + 2C_{pp}^0 S_{pp}^0(p_1, \epsilon_1). \end{aligned} \tag{3}$$

Here, C_{ab}^α are the nuclear contacts, that measure the probability to find a proton-proton (pp) pair or a proton-neutron (pn) pair close together, with quantum numbers denoted by α, while the functions S_{ab}^α are the contributions of these pairs to the spectral function. $\alpha = 1$ corresponds to the spin-one deuteron quantum numbers, and $\alpha = 0$ corresponds to the spin-zero s-wave quantum numbers. These are the main two-body channels of nuclear SRC pairs [23]. Based on the experience with the one-body momentum distribution [23], Eq. (3) is expected to be valid for $p_1 > p_F$. The probability to find a proton with energy ϵ_1 and large momentum p_1, has contribution from both pp and pn pairs. The equivalent neutron spectral function is obtained by changing between n and p.

The derivation of Eq. (3) starts with the definition of the spectral function

$$\begin{aligned} S^N(\boldsymbol{p}_1, \epsilon_1) = {} & \bar{\sum_i} \sum_{s_1, f} \delta(\epsilon_1 + E_f^{A-1} - E_i^A) \\ & \times \left| \langle \Psi_f^{A-1} | a_{\boldsymbol{p}_1, s_1} | \Psi_i^A \rangle \right|^2 \end{aligned} \tag{4}$$

where Ψ_i^A is the ground state wave function, $E_i^A = (Am - B_i^A)$ is the ground state energy and B_i^A is its binding energy, Ψ_f^{A-1} is an $(A-1)$-body eigenstate of the nuclear Hamiltonian with energy E_f^{A-1}, and $\bar{\sum}_i$ is an average over the magnetic projections of the ground state. m is the nucleon mass and $a_{\boldsymbol{p}_1, s_1}$ is the annihilation operator of a nucleon N with momentum $\boldsymbol{p}_1$ and spin s_1. S^p and S^n are normalized to the total number of protons and neutrons in the nucleus, correspondingly, i.e., $\int d\epsilon_1 \frac{d^3 p_1}{(2\pi)^3} S^p(\boldsymbol{p}_1, \epsilon_1) = Z$.

For $p_1 \longrightarrow \infty$, neglecting three-body or higher correlations, the ground state wave function is dominated by an SRC pair with very large relative momentum $\boldsymbol{p}_{12} = (\boldsymbol{p}_1 - \boldsymbol{p}_2)/2$ and can be written as

$$\Psi_i^A \xrightarrow[p_{12} \to \infty]{} \sum_\alpha \tilde{\varphi}_{12}^\alpha(\boldsymbol{p}_{12}) \tilde{A}_{12}^\alpha(\boldsymbol{P}_{12}, \{\boldsymbol{p}_k\}_{k \neq 1,2}). \tag{5}$$

This is the basic assumption of the contact theory, and it was validated using ab-initio calculations [23,33]. $\tilde{\varphi}_{ab}^\alpha$ are universal two-body functions, while $\tilde{A}_{ab}^\alpha$ describe the motion of the rest of the particles, and the pair's center of mass (CM) motion, $\boldsymbol{P}_{12} = \boldsymbol{p}_1 + \boldsymbol{p}_2$. In this picture, once particle 1 is removed, particle 2 is left with high momentum and can be treated as a spectator. Consequently, we may write

$$\Psi_f^{A,12} \equiv a_{\boldsymbol{p}_1, s_1}^\dagger \Psi_f^{A-1} = \mathcal{N} \hat{\mathcal{A}} \left\{ \Psi_f^{A-2} | \boldsymbol{p}_1 s_1; \boldsymbol{p}_2 s_2 \rangle \right\}. \tag{6}$$

Here, Ψ_f^{A-2} is an eigenstate of the $(A-2)$-body nuclear Hamiltonian with energy E_f^{A-2}, s_i is the spin of particle i, $\hat{\mathcal{A}}$ is the anti-symmetrizing operator, and $\mathcal{N}$ normalization factor. It follows that

$$E_f^{A-1} = \epsilon_2 + (A-2)m - B_f^{A-2} + \frac{\boldsymbol{P}_{12}^2}{2m(A-2)} \tag{7}$$

where $\epsilon_2 = \sqrt{p_2^2 + m^2}$ is the energy of the second correlated nucleon, B_f^{A-2} is the binding energy of the $(A-2)$-nucleon system, and the last term is the contribution of the CM motion of the $(A-2)$-nucleon system.

Substituting Eqs. (5) and (6) into Eq. (4), and assuming that the $(A-2)$-nucleon binding energy is narrowly distributed around a central value $\bar{B}_f^{A-2}$, we arrive at Eq. (3). For pairs of nucleons ab, the SRC functions S_{ab}^α are given by

$$S_{ab}^\alpha = \frac{1}{4\pi} \int \frac{d\boldsymbol{p}_2}{(2\pi)^3} \delta(f(\boldsymbol{p}_2)) \left| \tilde{\varphi}_{ab}^\alpha(|(\boldsymbol{p}_1 - \boldsymbol{p}_2)/2|) \right|^2 n_{ab}^\alpha(\boldsymbol{p}_1 + \boldsymbol{p}_2) \tag{8}$$

and

$$f(\boldsymbol{p}_2) = \epsilon_1 + \epsilon_2 - 2m + (B_i^A - \bar{B}_f^{A-2}) + \frac{(\boldsymbol{p}_1 + \boldsymbol{p}_2)^2}{2m(A-2)}, \tag{9}$$

where $n^{\alpha}_{ab}(\boldsymbol{P})$, the CM momentum distribution of the SRC pair, is given by $C^{\alpha}_{ab} n^{\alpha}_{ab}(\boldsymbol{P}) = \langle \tilde{A}^{\alpha}_{ab}(\boldsymbol{P}) | \tilde{A}^{\alpha}_{ab}(\boldsymbol{P}) \rangle$. In practice, it can be assumed that all SRC pairs have similar CM distribution $n_{CM}(\boldsymbol{P})$, which we shall take as a three-dimensional Gaussian with a width σ_{CM} [28,34,35]. The spectral functions S^{α}_{ab} are expected to be almost identical across the table of nuclides, as the CM and binding energy corrections are relatively small for nuclei heavier than ^{12}C [28].

The delta function in Eq. (8) can be used to eliminate the integration over the angles, and S^{α}_{ab} can be obtained through numerical integration over p_2, without further approximations. In this integration we also require that $|(\boldsymbol{p}_1 - \boldsymbol{p}_2)/2| > p_F$. Alternatively, we can continue analytically if we replace the CM term of Eq. (9) by its mean value $\bar{T}^{A-2}_{CM} = \langle P^2_{12} \rangle / 2m(A-2) = 3\sigma^2_{CM}/2m(A-2)$. This should be a good approximation for small values of σ_{CM} or large values of A. Then, the delta function can be used to fix the magnitude of $\boldsymbol{p}_2$, given by

$$p^0_2(\epsilon_1) = \sqrt{\left[2m - \epsilon_1 - (B^A_i - \bar{B}^{A-2}_f) - \bar{T}^{A-2}_{CM}\right]^2 - m^2}. \tag{10}$$

We can also see that if the CM momentum distribution $n_{CM}(\boldsymbol{P})$ has a zero width, i.e. n_{CM} is a delta function which dictates $\boldsymbol{p}_2 = -\boldsymbol{p}_1$, the spectral function becomes simply a delta function, centered around

$$\epsilon_1 = 2m - \sqrt{p^2_1 + m^2} - (B^A_i - \bar{B}^{A-2}_f). \tag{11}$$

According to Eq. (10), the momentum magnitude p_2 of the second-emitted nucleon in $A(e,e'pN)$ experiments depends only on the initial energy ϵ_1 but not on the initial momentum p_1 of the knocked-out proton. This might not seem reasonable at first glance, since we expect that $\boldsymbol{p}_2 \approx -\boldsymbol{p}_1$ [5,6]. But, if one substitutes the value of ϵ_1 of Eq. (11) together with $\bar{T}^{A-2}_{CM} = 0$, into Eq. (10), we obtain $p^0_2 = p_1$, as expected. For a given p_1, the value of ϵ_1 of Eq. (11) should be close to a maximum point in the spectral function, and thus most experimental data is centered around such values of p_1 and ϵ_1, leading to the observation of $\boldsymbol{p}_2 \approx -\boldsymbol{p}_1$. If sufficient experimental data of exclusive experiments in other domains of the momentum-energy plane will be available, it might be possible to see the energy dependence of p^0_2 and compare it to Eq. (10). We expect for corrections to this relation due finite A, the distribution of the B^{A-2}_f around the mean value $\bar{B}^{A-2}_f$, and FSI effects.

To calculate the spectral function we must first calculate the universal functions $\tilde{\varphi}^{\alpha}_{ab}(\boldsymbol{p})$. These are the zero-energy solutions of the two-body Schrodinger equation for the spin-zero $\alpha = 0$ channel, and the deuteron wave-function for $\alpha = 1$. In Fig. 1 we present the resulting functions using the AV18 nucleon-nucleon (NN) potential [36] and the chiral EFT NN force N3LO(600) [37] for the pp spin-zero channel and the pn deuteron channel. It can be seen that the two potentials produce similar functions up to the cutoff value of the N3LO potential ($p \approx 3$ fm^{-1}). Some differences in the pp functions, like the location of the node, are observed.

Before presenting our calculations for the spectral function, we note that $n_{CM}(\boldsymbol{P})$ is expected to have a narrow distribution around zero, in each axis, with $\sigma_{CM} \approx p_F/2$. Therefore, the main contribution to the spectral function comes from $\boldsymbol{p}_2$ being anti-parallel to $\boldsymbol{p}_1$. As can be seen in Fig. 1, the pp function has a node around $p_{node} \approx 2$ fm^{-1}, and thus we expect S^0_{pp} to have a minimum for

$$\frac{p_1 + p^0_2(\epsilon_1)}{2} = p_{node}. \tag{12}$$

The calculations of S^1_{pn} and S^0_{pp}, based on Eqs. (8) and (9), are presented in Figs. 2 and 3, using the AV18 NN interaction. In Fig. 2,

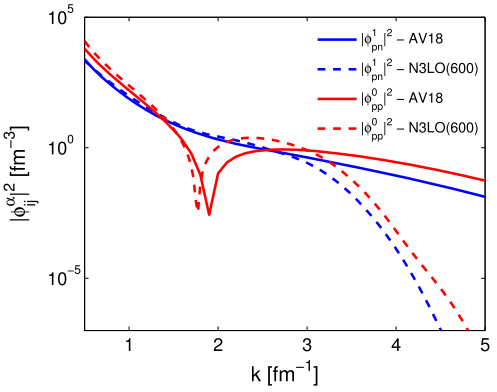

Fig. 1. The universal two-body functions calculated using two different potentials, for deuteron pn pairs and s-wave pp pairs. The functions are normalized such that $\int_{p_F}^{\infty} |\varphi^{\alpha}_{ab}|^2 d\boldsymbol{p}/(2\pi)^3 = 1$.

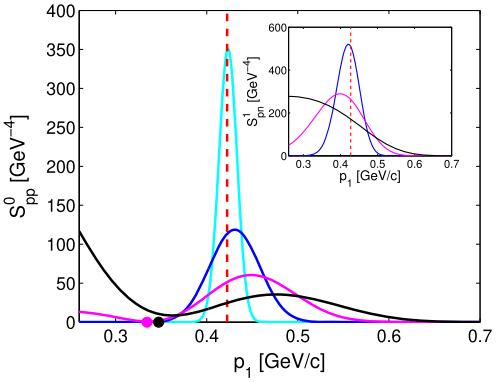

Fig. 2. S^0_{pp} of ^{4}He as a function of p_1 for fixed $\epsilon_1 = 0.82$ GeV/c, using the AV18 potential and different values of σ_{CM}: 10 MeV (cyan), 30 MeV (blue), 60 MeV (magenta) and 100 MeV (black). The dashed red line is the back-to-back prediction of Eq. (11), and the black and magenta points are the estimated location of the minimum of S^0_{pp} based on Eq. (12). Inset: the results for S^1_{pn} for $\sigma_{CM} = 30$, 60 and 100 MeV.

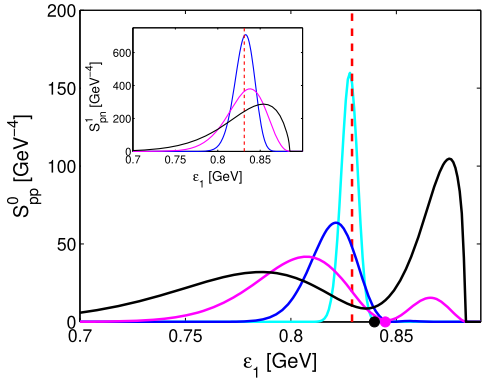

Fig. 3. The same as in Fig. 2, but as a function of ϵ_1 for fixed $p_1 = 400$ MeV/c.

they are presented as a function of p_1, at $\epsilon_1 = 0.82$ GeV/c and different values of σ_{CM}. In Fig. 3, the calculations are a function of ϵ_1 at $p_1 = 400$ MeV/c. The calculations were done for ^{4}He, taking B^A_i to be its binding energy and $\bar{B}^{A-2}_f$ the binding energy of the deuteron for the pn case and zero for the pp case. We note that the experimental extraction of σ_{CM} of ^{4}He is 100 ± 20 MeV [8,28], in a good agreement with available theoretical estimations [34,35].

Calculations for heavier nuclei are similar, with ϵ_1 shifted due to the different values of B^A_i and $\bar{B}^{A-2}_f$. Similar calculations using the N3LO(600) potential are presented in the supplemental ma-

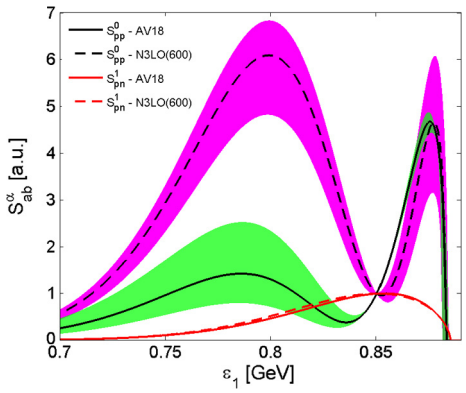

Fig. 4. S^0_{pp} and S^1_{pn} for ^{4}He as a function of ϵ_1 for fixed $p_1 = 400$ MeV/c, normalized to 1 at $\epsilon_1 = 0.85$ GeV. The solid and dashed black (red) lines correspond to S^0_{pp} (S^1_{pn}) for the AV18 and N3LO(600) potentials, respectively. The bands around the black lines show the effect of changing the value of p_1 between $390 - 410$ MeV/c. The corresponding bands for the red lines are much narrower and are not shown here.

terials. It can be seen that for small values of σ_{CM}, the spectral function is very close to the zero-CM prediction of Eq. (11), corresponding to back-to-back SRC pairs. As the CM width is increased, S^α_{ab} deviates from this back-to-back picture. In addition, we can see that the pp spectral function has an interesting structure as it develops two maxima for $\sigma_{CM} > 60$ MeV/c. This structure reflects the node in the pp function, as predicted in Eq. (12).

To compare between the results of the AV18 and N3LO(600) potentials, we present in Fig. 4 the ^{4}He calculations of S^1_{pn} and S^0_{pp}, as a function of ϵ_1 for fixed $p_1 = 400$ MeV/c and $\sigma_{CM} = 100$ MeV/c. Here, the results are normalized to 1 at $\epsilon_1 = 0.85$ GeV. The bands around the S^0_{pp} results show the effect of changing the value of p_1 between $390 - 410$ MeV. It is clear that the S^1_{pn} results are very similar for the two potentials, while the results for S^0_{pp} show significant differences. This is due to the differences seen in the pp functions presented in Fig. 1 around their node. Based on this sensitivity of S^0_{pp} to the potential, it might be possible to constrain the short-range part of the NN potential using SRCs experimental data, as we will further discuss below. We note that S^0_{pp} becomes less sensitive to the potential for higher or lower values of p_1.

It should be noted that our expressions for the spectral function derived from the contact formalism are similar to the convolution model presented by Ciofi degli Atti et al. in [34,38], and revisited recently in [39,40]. The convolution model was shown to agree with ab initio calculations of the spectral function of ^{3}He [39]. Nevertheless, our model differs slightly from the convolution model. The contact formalism allows us, in principle, to take into account contributions from all two-body channels. In this work, we consider the two leading np two-body functions, as opposed to a single deuteron function used in the convolution model. The main contribution comes from the deuteron channel, and we expect the additional np channel to have an effect of about 10%. Another small difference is the integration domain of Eq. (8), where we included the constrain $|(\boldsymbol{p}_1 - \boldsymbol{p}_2)/2| > p_F$, while in the recent calculations of Ref. [39] a slightly different constrain was introduced, leading to a similar effect. Additionally, we use the experimental CM distributions, as opposed to the ab-initio CM distributions used in the convolution model. Notice also that we use relativistic expressions for the energy while the convolution model is completely non-relativistic. A direct comparison between the two models is presented in the supplemental materials, showing a good agreement for ^{4}He and some differences for ^{12}C. The contact formalism was also shown to agree with ab-initio calculations of momentum and coordinate-space distributions [23].

Equipped with our contact relation for the spectral function, we can go back to the exclusive electron-scattering experiments. One of the main results of these experiments is the ratio between the number of emitted pp pairs and pn pairs, extracted from the $A(e,e'pp)$ and $A(e,e'pn)$ cross sections. Based on Eq. (3), we can see that if there is a proton in some nucleus A with off-shell energy ϵ_1 and momentum $p_1 > k_F$, then it is part of an SRC pair, which is either a pp pair or a pn pair. The ratio of the number of such pp to pn pairs is given by

$$\frac{\#pp}{\#pn}(p_1,\epsilon_1) = \frac{C^0_{pp} S^0_{pp}(p_1,\epsilon_1)}{C^1_{pn} S^1_{pn}(p_1,\epsilon_1) + C^0_{pn} S^0_{pn}(p_1,\epsilon_1)}. \tag{13}$$

For symmetric nuclei ($N = Z$) we expect that $C^0_{pp} = C^0_{pn} \equiv C^0$ [23], and thus this ratio depends only on a single parameter C^1_{pn}/C^0. We can see that this ratio generally depends on both the initial momentum of the proton p_1 and its energy ϵ_1. Within the PWIA, and based on Eq. (2), this ratio can be extracted from the exclusive-scattering experiments and is given by $A(e,e'pp)/2A(e,e'pn)$.

The relation of the measured nucleon knockout cross-section ratios to PWIA calculations and ground-state energy-momentum densities relies on the fact that for the high-Q^2 kinematics used in the measurement, according to calculations, reaction mechanisms other than the hard breakup of SRC pairs are suppressed and any residual effects are significantly reduced when considering cross-section ratios as oppose to absolute cross-sections [18,41–44]. The cancellation of reaction mechanisms in the cross-section ratio steams from the approximate factorization of the experimental cross-section at high-Q^2, which also allows correcting the data for any remaining effects of FSI and Single-Charge Exchange (SCX) of the outgoing nucleons using an Eikonal approximation in a Glauber framework [19,35,45,46]. The experimental data discussed in this work is already corrected for such effects [7–9,27]. It should be noted that these corrections were verified experimentally, see discussion in [18,41,43,46–49].

The $\#pp/\#pn$ ratio was extracted from exclusive-scattering experimental data for ^{4}He [8] and ^{12}C [7,27]. In these experiments, the main focus was the dependence of these ratios on the initial momentum p_1, and not the dependence on ϵ_1. In both experiments, the ratios were measured in several kinematical settings, each corresponding to specific central values of p_1 and ϵ_1. The momentum-dependence of the ratio was highlighted, but the effects of the initial energy ϵ_1 were not discussed. This discussion is also missing in previous theoretical works that used the momentum distribution as a starting point to predict the $\#pp/\#pn$ ratio [23,33,50,51]. The study of this ratio, and SRC pairs in general, should be extended to include the full energy and momentum (ϵ_1, p_1) dependence.

Using Eq. (13) we can predict the value of the $\#pp/\#pn$ ratio as a function of both p_1 and ϵ_1, for any nucleus, if the values of the contacts and σ_{CM} for this nucleus are known. The values of the contacts for several nuclei with mass number up to $A \leq 40$ were extracted recently [23] using variational Monte Carlo (VMC) two-body densities in momentum and coordinate space [16,52], calculated using the AV18 NN potential and the Urbana X (UX) three-nucleon force [53]. We will focus here on ^{4}He and ^{12}C, for which the experimental data is also available. As mentioned before, for symmetric nuclei as these, the $\#pp/\#pn$ ratio depends only on one contact ratio. We use the available experimental data of Refs. [8] to fit this ratio of contacts for ^{4}He, utilizing Eq. (13). For ^{12}C, we fit the ratio of contacts to the $\#pp/\#p$ ratio of Ref. [27], which will be discussed below. The fitted values for ^{4}He and ^{12}C

Table 1
The fitted values of the contact ratio C^1_{pn}/C^0 for ^{4}He and ^{12}C. The rows correspond to different potentials and the columns correspond to different fits. $(e,e'pN)$ is the fit to the experimental $\#pp/\#pn$ ratio of Ref. [8] for ^{4}He, and to $\#pp/\#p$ of Ref. [27] for ^{12}C, presented in this work. The k-VMC and r-VMC are fits to VMC two-body densities in momentum and coordinate space, respectively, taken from Ref. [23]. Only the values in the $(e,e'pN)$ column are used in this paper.

A	Potential	$(e,e'pN)$	k-VMC	r-VMC
^{4}He	AV18	20 ± 5	18.4 ± 0.8	20.5 ± 0.2
	N3LO(600)	33 ± 8	–	–
	N2LO(1.0)	19 ± 5	–	–
	N2LO(1.2)	15 ± 4	–	–
^{12}C	AV18	14 ± 3	12.5 ± 2	18.0 ± 0.2
	N3LO(600)	25 ± 5	–	–
	N2LO(1.0)	19 ± 4	–	–
	N2LO(1.2)	20 ± 5	–	–

are given in Table 1, using the AV18, the N3LO(600) and the local chiral N2LO [54,55] potentials, for the calculation of the spectral function, the experimental estimate $\sigma_{CM}(^4\text{He}) = 100$ MeV [8], and $\sigma_{CM}(^{12}\text{C}) = 143$ MeV [5,27,28], and the relevant bound-state energies for B^A_i and $\bar{B}^{A-2}_f$. The local N2LO chiral potential includes two cutoffs, $R = 1.0$ fm and $R = 1.2$ fm, denoted here by N2LO(1.0) and N2LO(1.2), respectively. Previously extracted contact values, using the AV18 NN potential and the UX three-body force, are also given in the table, and agree with the AV18 ratio extracted here. This ratio of contacts C^1_{pn}/C^0 gives us the ratio between the total number of SRC pn pairs in the deuteron channel and the number of SRC pp pairs. Only the values in the first column of Table 1 are used in the reminder of this paper.

The extracted contact ratio using N3LO(600), also shown in Table 1, is larger than the one obtained using AV18, which shows that this ratio is model dependent. The main source for this model dependence is the sharp fall of the N3LO(600) $|\tilde{\varphi}^{\alpha}_{ab}|^2$ functions for $p > 3$ fm^{-1} (Fig. 1). This reduces significantly the number of SRC pp pairs, i.e. the value of C^0_{pp}, because the contribution of $p > 3$ fm^{-1} is small, while the AV18 pp function has significant contribution to SRC pairs for $p > 3$ fm^{-1}. We can look on the total number of pn deuteron pairs over pp pairs with relative momentum restricted to $p_F < p < p_{max} \equiv 3$ fm^{-1}, given by

$$\frac{C^1_{pn}\int_{p_F}^{p_{max}} d\boldsymbol{p}|\tilde{\varphi}^1_{pn}(\boldsymbol{p})|^2}{C^0_{pp}\int_{p_F}^{p_{max}} d\boldsymbol{p}|\tilde{\varphi}^0_{pp}(\boldsymbol{p})|^2}. \tag{14}$$

For AV18 we get a ratio of 32 ± 8 for ^{4}He, which is much larger than the ratio of all $p > p_F$ pairs of Table 1. For N3LO(600) we get a ratio of 35 ± 9 for ^{4}He, similar to the original ratio shown in the table. We can see that the two potentials give consistent values when restricting the momentum range to $p_F < p < 3$ fm^{-1}, and the model dependence disappears. Similar result is obtained also for ^{12}C. In this discussion, it is important to distinguish between two $\#pp/\#pn$ SRC ratios. One is measured in exclusive scattering, given by Eq. (13), and depends on both the initial momentum p_1 and the initial energy ϵ_1 of the knocked out proton. The second, describes the number of pp and pn (deuteron) pairs with relative momentum p, and is given by $C^0_{pp}|\tilde{\varphi}^0_{pp}(p)|^2/C^1_{pn}|\tilde{\varphi}^1_{pn}(p)|^2$.

Regarding the local chiral interactions, for ^{4}He, the "hardest" chiral interaction, N2LO(1.0), results in a contact ratio that is very similar to that of the phenomenological AV18 interaction. Increasing its cutoff to 1.2 fm slightly reduces the contact ratios. As mentioned above, the softer non-local N3LO(600) interaction produces a larger contact ratio. For ^{12}C, the cutoff dependence of the N2LO interaction is somewhat less pronounce and they both agree, within uncertainties, with the AV18 extraction. As discussed

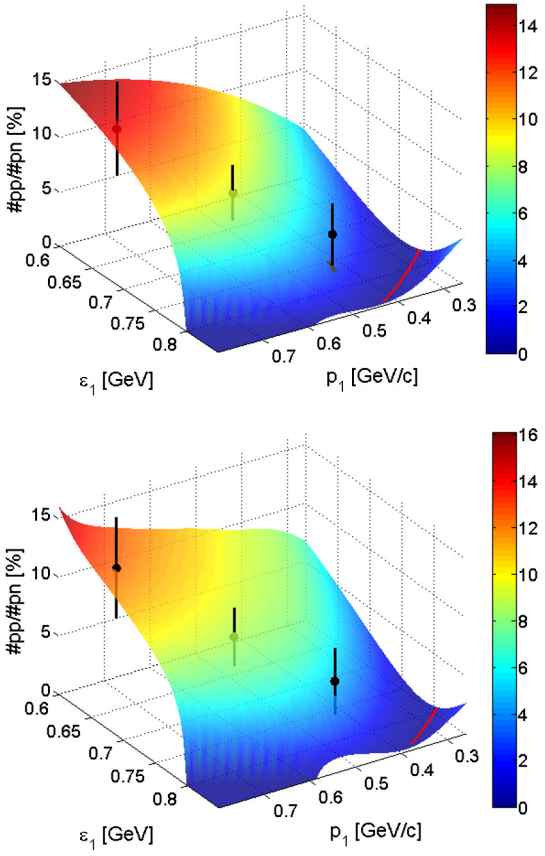

Fig. 5. (Top) The ^{4}He $\#pp/\#pn$ ratio as a function of both p_1 and ϵ_1, according to Eq. 13 and the contact ratio fitted in this work (Table 1), using the AV18 potential. The red line is the analytic prediction for a minimal ratio value, and the black points are the experimental data of Ref. [8]. The location of experimental points that do not intersect the surface are indicated by a gray patch on the surface. (Bottom) The same but using the N3LO(600) potential. The values of the experimental data in the momentum and energy axes are $p_1 = 0.49 \pm 0.1,\ 0.62 \pm 0.09,\ 0.75 \pm 0.08$ GeV/c and $\epsilon_1 = 0.81^{+0.09}_{-0.21},\ 0.74^{+0.11}_{-0.19},\ 0.66^{+0.09}_{-0.21}$ GeV, respectively.

before, some of these differences can be attributed to the differences in the universal functions, which depend on the potential. Model-independence is expected for contact ratios of two nuclei, for the same interaction and two-body channel, as observed in Refs. [56,57], but not for the ratios presented in Table 1. Decisive conclusion regarding such model independence is not possible here, due to the relatively large uncertainties in the extracted contact values.

Using the fitted contact ratio for ^{4}He, we can now predict the full dependence of the $\#pp/\#pn$ ratio. The results are presented in Fig. 5 using the AV18 and N3LO(600) potential. We can see that the surface describes well the exclusive-scattering experimental data of Ref. [8] (the black points) using both potentials. We also include our analytic prediction for the (p_1, ϵ_1) points for which the $\#pp/\#pn$ ratio is minimal (red line), based on Eq. (12). There is a good agreement with the full numerical calculations. One can see that the available experimental data sits on a diagonal line in the (p_1, ϵ_1) plane, while there is no experimental data for substantial parts of this plane. Thus, additional experimental data, covering the (p_1, ϵ_1) plane, is needed to fully investigate the theoretical predictions presented in Fig. 5.

Based on Fig. 5, it seems that AV18 and N3LO(600) predict a similar structure for $\#pp/\#pn$. This takes us back to Fig. 4, which showed that S^0_{pp} is sensitive to the NN potential around $p_1 = 400$ MeV. Thus, if the number of SRC pp pairs will be measured in future exclusive experiments as a function of ϵ_1 with

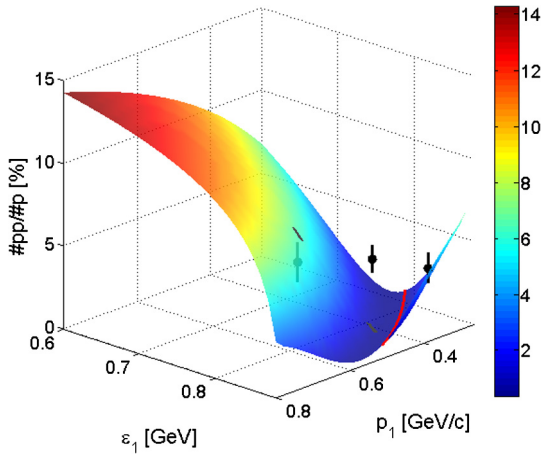

Fig. 6. The same as in Fig. 5, but for the ^{12}C $\#pp/\#p$ ratio, according to Eq. (15), using the AV18 potential. The black points are the experimental data of Ref. [27]. The values of the experimental data in the momentum and energy axes are $p_1 = 0.35 \pm 0.05,\ 0.45 \pm 0.05,\ 0.55 \pm 0.05$ GeV/c and $\epsilon_1 = 0.86^{+0.04}_{-0.11},\ 0.84^{+0.05}_{-0.15},\ 0.79^{+0.11}_{-0.14}$ GeV, respectively.

fixed $p_1 = 400$ MeV, it might be possible to use it to constrain the NN potential. Since we are discussing pp pairs with high relative momentum, it should be sensitive to the short distance part of the potential. Based on the bands presented in Fig. 5, we note that the experimental uncertainty of the value of p_1 should not be larger than 10 MeV, in order to differentiate between AV18 and N3LO(600).

One can also consider the $\#pp/\#p$ ratio, i.e. the number of correlated pp pairs consisting of a proton with off-shell momentum-energy (p_1, ϵ_1), divided by the total number of such protons. For $p_1 > k_F$, this ratio should be given by

$$\frac{\#pp}{\#p}(p_1, \epsilon_1) = \frac{C^0_{pp} S^0_{pp}}{2C^0_{pp} S^0_{pp} + C^1_{pn} S^1_{pn} + C^0_{pn} S^0_{pn}}. \tag{15}$$

This ratio was extracted from exclusive scattering experiments for ^{4}He [8] and ^{12}C [27]. We note that similar corrections to those discussed above (for FSI and SCX) were already applied to the cross sections to obtain the experimental $\#pp/\#p$ ratio. These corrections are much more significant here, comparing to the $\#pp/\#pn$ corrections, and include transparency effects and significant model-dependent acceptance corrections (of the order of a factor of 10 for the experimental data analyzed here).

Fig. 6 depicts the $\#pp/\#p$ ratio for ^{12}C using the AV18 potential, based on Eq. (15) and the contact ratio fitted in this work (Table 1), compared to the experimental data of Ref. [27]. Here, one can see that while the theory predicts deep minima in the ratio, the experimental data seems to show a constant ratio of about 5%. Similar figure is presented in the supplemental materials using the N3LO(600) potential. There are few possible explanations for this disagreement between our theory and the data. As mentioned above, the corrections applied to the data in order to obtain the $\#pp/\#p$ ratio are quite significant. The disagreement shown in Fig. 6 might indicate that these corrections should be re-examined. Experimental data which requires smaller corrections can be useful here, for example using large-acceptance detectors (see e.g. Ref. [9]). It is also possible that the limited statistics and the large bins of the data presented in Fig. 6 smears the finer details of the $\#pp/\#p$ ratio, yielding approximately a constant ratio. If this is the case, to verify the theoretical predictions of this work, better data is needed. Finally, corrections to the theory should also be studied, such as the effects of the energy distribution of the $A-2$ system (B_f^{A-2}) around its mean value.

In the supplemental materials, we present the $\#pp/\#p$ ratio also for ^{4}He and the $\#pp/\#pn$ ratio for ^{12}C, using the same values of the contacts (Table 1). Similar to ^{12}C, the experimental data for the $\#pp/\#p$ ratio of ^{4}He [8] seems to indicate a constant value for the ratio, while the theory shows a different picture. The single experimental point for the ^{12}C $\#pp/\#pn$ ratio is in agreement with the theoretical predictions. The analysis of the $\#pn/\#p$ ratio is also presented in the supplemental materials for ^{4}He and ^{12}C. The experimental data for this ratio [7,8] includes quite large errorbars and better data is needed to investigate the theoretical predictions. Similar analysis using the local chiral N2LO potential is also presented in the supplementary.

To summarize, the nuclear contact formalism was used to derive a relation between the nuclear contacts, describing the probability to find SRC pairs in the nucleus, and the spectral function. This relation was utilized to analyze the $\#pp/\#pn$, $\#pp/\#p$ and $\#pn/\#p$ ratios for ^{4}He and ^{12}C, emphasizing the full dependence in the (p_1, ϵ_1) plane and revealing a richer structure than was assumed so far, using few different nuclear potentials. For $\#pp/\#pn$ there is a good agreement with the available experimental data, extracted from exclusive electron-scattering experiments, while for $\#pp/\#p$ there seems to be a disagreement. Possible explanations for this disagreement were discussed. Better experimental data is needed for $\#pn/\#p$ in order to compare with the theoretical predictions. The contact ratio C^1_{pn}/C^0 for ^{4}He and ^{12}C extracted using the AV18 potential agrees with previous values, extracted using the same potential. The contact values seem to depend on the NN interaction, but this model dependence is resolved if one is looking on a limited high-momentum range. It was also shown that the contribution of SRC pp pairs to the spectral function is sensitive to the NN potential, which can be used to constrain the short-range part of the potential, if appropriate experimental data is available.

A main conclusion of this work is that the full energy and momentum dependence of exclusive electron-scattering experiments should be studied, experimentally and theoretically, in order to obtain a full picture regarding nuclear SRCs. Further experimental data for the $\#pp/\#pn$, $\#pp/\#p$ and $\#pn/\#p$ ratios and other observables, for different nuclei, covering the energy-momentum plane, is required for investigating the predictions presented in this work.

Acknowledgements

This work was supported by the PAZY Foundation, the Israel Science Foundation under grant number 1334/16 and by the Office of Nuclear Physics of the U.S. Department of Energy under grant Contract Numbers DE-FG02-94ER40818.

Appendix A. Supplementary material

Supplementary material related to this article can be found online at https://doi.org/10.1016/j.physletb.2019.02.019.

References

[1] L.L. Frankfurt, M.I. Strikman, D.B. Day, M. Sargsyan, Phys. Rev. C 48 (1993) 2451.
[2] K. Egiyan, et al., Phys. Rev. C 68 (2003) 014313.
[3] K. Egiyan, et al., Phys. Rev. Lett. 96 (2006) 082501.
[4] N. Fomin, et al., Phys. Rev. Lett. 108 (2012) 092502.
[5] A. Tang, et al., Phys. Rev. Lett. 90 (2003) 042301.
[6] E. Piasetzky, M. Sargsian, L. Frankfurt, M. Strikman, J.W. Watson, Phys. Rev. Lett. 97 (2006) 162504.
[7] R. Subedi, et al., Science 320 (2008) 1476.
[8] I. Korover, et al., Phys. Rev. Lett. 113 (2014) 022501.
[9] O. Hen, et al., CLAS Collaboration, Science 346 (2014) 614.
[10] H. Baghdasaryan, et al., Phys. Rev. Lett. 105 (2010) 222501.
[11] M. Duer, et al., CLAS Collaboration, arXiv:1810.05343, 2018.

[12] R. Schiavilla, R.B. Wiringa, Steven C. Pieper, J. Carlson, Phys. Rev. Lett. 98 (2007) 132501.
[13] M. Alvioli, C. Ciofi degli Atti, H. Morita, Phys. Rev. Lett. 100 (2008) 162503.
[14] H. Feldmeier, W. Horiuchi, T. Neff, Y. Suzuki, Phys. Rev. C 84 (2011) 054003.
[15] M. Alvioli, C. Ciofi degli Atti, L.P. Kaptari, C.B. Mezzetti, H. Morita, Phys. Rev. C 87 (2013) 034603.
[16] R.B. Wiringa, R. Schiavilla, S.C. Pieper, J. Carlson, Phys. Rev. C 89 (2014) 024305.
[17] M. Sargsian, T.V. Abrahamyan, M.I. Strikman, L.L. Frankfurt, Phys. Rev. C 71 (2005) 044615.
[18] O. Hen, G.A. Miller, E. Piasetzky, L.B. Weinstein, Rev. Mod. Phys. 89 (2017) 045002.
[19] C. Ciofi degli Atti, Phys. Rep. 590 (2015) 1.
[20] R. Weiss, B. Bazak, N. Barnea, Phys. Rev. Lett. 114 (2015) 012501.
[21] R. Weiss, B. Bazak, N. Barnea, Phys. Rev. C 92 (2015) 054311.
[22] R. Weiss, N. Barnea, Phys. Rev. C 96 (2017) 041303(R).
[23] R. Weiss, R. Cruz-Torres, N. Barnea, E. Piasetzky, O. Hen, Phys. Lett. B 780 (2018) 211.
[24] R. Weiss, B. Bazak, N. Barnea, Eur. Phys. J. A 52 (2016) 92.
[25] R. Weiss, E. Pazy, N. Barnea, Few-Body Syst. 58 (2017) 9.
[26] R. Cruz-Torres, et al., Phys. Lett. B 785 (2018) 304.
[27] R. Shneor, et al., Phys. Rev. Lett. 99 (2007) 072501.
[28] E.O. Cohen, et al., CLAS Collaboration, Phys. Rev. Lett. 121 (2018) 092501.
[29] M. Duer, et al., CLAS Collaboration, Nature 560 (2018) 617.
[30] T. De Forest, Nucl. Phys. A 392 (1983) 232.
[31] L. Frankfurt, M. Strikman, Phys. Rep. 160 (1988) 235.
[32] L. Frankfurt, M.M. Sargsian, M. Strikman, Int. J. Mod. Phys. A 23 (2008) 2991.
[33] M. Alvioli, C. Ciofi degli Atti, H. Morita, Phys. Rev. C 94 (2016) 044309.
[34] C. Ciofi degli Atti, S. Simula, Phys. Rev. C 53 (1996) 1689.
[35] C. Colle, W. Cosyn, J. Ryckebusch, M. Vanhalst, Phys. Rev. C 89 (2014) 024603.
[36] R.B. Wiringa, V.G.J. Stoks, R. Schiavilla, Phys. Rev. C 51 (1995) 38.
[37] E. Epelbaum, H.-W. Hammer, U.-G. Meißner, Rev. Mod. Phys. 81 (2009) 1773.
[38] C. Ciofi degli Atti, S. Simula, L.L. Frankfurt, M.I. Strikman, Phys. Rev. C 44 (1991) R7(R).
[39] C. Ciofi degli Atti, C.B. Mezzetti, H. Morita, Phys. Rev. C 95 (2017) 044327.
[40] C. Ciofi degli Atti, H. Morita, Phys. Rev. C 96 (2017) 064317.
[41] J. Arrington, D.W. Higinbotham, G. Rosner, M. Sargsian, Prog. Part. Nucl. Phys. 67 (2012) 898.
[42] C. Colle, et al., Phys. Rev. C 92 (2015) 024604.
[43] C. Colle, W. Cosyn, J. Ryckebusch, Phys. Rev. C 93 (2016) 034608.
[44] W.U. Boeglin, et al., Phys. Rev. Lett. 107 (2011) 262501.
[45] L.L. Frankfurt, M.M. Sargsian, M.I. Strikman, Phys. Rev. C 56 (1997) 1124.
[46] D. Dutta, K. Hafidi, M. Strikman, Prog. Part. Nucl. Phys. 69 (2013) 1.
[47] O. Hen, et al., CLAS Collaboration, Phys. Lett. B 722 (2013) 63.
[48] L. Frankfurt, M. Strikman, M. Zhalov, Phys. Lett. B 503 (2001) 73.
[49] V.R. Pandharipande, S.C. Pieper, Phys. Rev. C 45 (1992) 791.
[50] J. Ryckebusch, et al., J. Phys. G, Nucl. Part. Phys. 42 (2015) 055104.
[51] T. Neff, H. Feldmeier, W. Horiuchi, Phys. Rev. C 92 (2015) 024003.
[52] D. Lonardoni, A. Lovato, S.C. Pieper, R.B. Wiringa, Phys. Rev. C 96 (2017) 024326.
[53] S.C. Pieper, V.R. Pandharipande, R.B. Wiringa, J. Carlson, Phys. Rev. C 64 (2001) 014001.
[54] A. Gezerlis, I. Tews, E. Epelbaum, S. Gandolfi, K. Hebeler, A. Nogga, A. Schwenk, Phys. Rev. Lett. 111 (2013) 032501.
[55] A. Gezerlis, I. Tews, E. Epelbaum, M. Freunek, S. Gandolfi, K. Hebeler, A. Nogga, A. Schwenk, Phys. Rev. C 90 (2014) 054323.
[56] R. Weiss, A. Schmidt, G.A. Miller, N. Barnea, Phys. Lett. B 790 (2019) 484.
[57] J.-W. Chen, W. Detmold, J.E. Lynn, A. Schwenk, Phys. Rev. Lett. 119 (2017) 262502.